Reinterpretation of displacements and failure mechanisms of the upper portion of Randa rock slide

Andrea Pedrazzini, Michel Jaboyedoff & Marc-Henri Derron
Institute of geomatics and risk analysis, University of Lausanne, Switzerland
Antonio Abellán & Carmen Vega Orozco
Institute of geomatics and risk analysis, University of Lausanne, Switzerland

ABSTRACT
The Randa rockslide (South-western Switzerland) is one of the most studied rockslides in the world. Different studies deal with the structural settings and the failure mechanism of the 1991 collapse. A potential unstable mass is still present in the upper part of the scar and is monitored since 1991 by different techniques. In this paper, after a review of previous studies, we focus on the use of new monitoring techniques for the reinterpretation of the kinematics of the unstable part. More specifically, the different displacements data have been reinterpreted and correlated to the structural setting. In addition, the potential unstable volume has been re-evaluated using a High Resolution DEM through the Sloping Local Base Level method, constrained by the main joints orientation.

RÉSUMÉ
Le glissement rocheux de Randa est l'un des glissement les plus étudié du monde. Plusieurs études ont été menées concernant les mécanismes de rupture des deux événements survenus en 1991. Une masse rocheuse potentiellement instable est encore présente dans la partie Nord de la niche d'arrachement de l'éboulement de 1991. La zone est surveillée depuis 1991 avec plusieurs techniques. Dans ce papier, après une synthèse des études précédentes effectuées sur la totalité du glissement, l'accent sera mis sur l'apport des nouvelles techniques numériques sur la surveillance des déplacements et l'interprétation de la cinématique de la zone actuellement instable. Le volume potentiellement instable a été évalué à l'aide du concept du niveau de base et contraint par une étude structurale menée sur la base d'un modèle numérique de terrain à haute résolution.

1 INTRODUCTION

The Randa rockslide, Wallis (western Switzerland), is one of the most studied rockslides in the world. In April 1991 a first large rockslides occurred involving 20 M of m^3. In May 1991, another rock mass of about 10 M of m^3 was released.

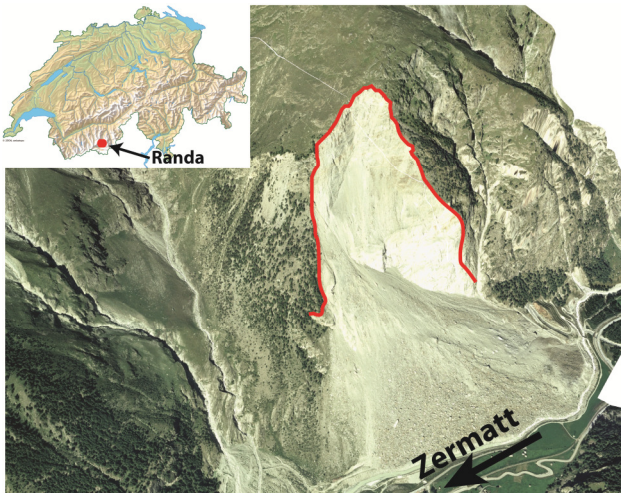

Figure 1. Geographical setting of the Randa rockslide.

From a geological point of view, the materials of the study area are: (a) competent orthogneiss characterized by a intense geological deformation and (b) paragneisses with dominant regional tectonic foliation dipping toward west. The structural properties and the failure mechanism of the 1991 rock slides have been extensively studied.
A potential unstable mass is still present in the upper part of the scar and is monitored since 1991 by different techniques. During the last 20 years, new monitoring techniques have been applied in order to better define the present-day kinematics and its possible evolution. In this paper, after a comprehensive review of the different monitoring techniques and the interpretations of the 1991 events and the upper potential unstable area, we focus on the impact and the improvement of the new monitoring techniques resulting of the previous mechanisms hypothesis. More specifically, the different displacements data have been reinterpreted and correlated to the structural setting. The potential unstable volume has been re-evaluated based on High Resolution Digital Elevation Model (HRDEM) techniques together with the *Sloping Local Base Level* method (Jaboyedoff et al., 2009).

2 PREVIOUS STUDIES

The previous studies could be divided into four main categories, corresponding to the different stages in the understanding of the slope instability.

2.1 Preliminary studies of the 1991 events

The investigations carried out during and just after the 1991 events mainly involved management of the crisis (Sartori et al., 2003). These analyses were focused on volume estimations, quick interpretations of the monitoring results and on the stability studies of the rockslide dam (Ischi et al., 1991; Pirocchi, 1992; Rouiller, 1992; Götz and Zimmermann, 1993). The first detailed analysis of the structural and geomechanical setting of the lower and upper parts of the slide were also performed and the first interpretations of the failure mechanism and the triggering factors were proposed by different authors (Wagner, 1991, Noverraz and Bonnard, 1992, Schindler et al. 1993).

2.2 Kinematics studies of the 1991 events

After the crisis management, researches have focused on the understanding of the kinematics of the 1991 events. The parameters controlling the 1991 collapse could be divided into two main categories: pre-existing factors and degrading factors (Sartori et al., 2003). For the first category, Sartori et al. (2003) indicate that the presence of a persistent fault at the base of the slope coupled with a steeply persistent joint is the major predisposing factors of the rockslide. Ground water circulation and the related mineralogical weathering (Girod et al., 1999, Jaboyedoff et al., 2004b) coupled with seismic activity are considered as the long term degrading factors (Schindler et al. 1993, Sartori et al., 2003). The ultimate triggering factor was identified as the important snow melting during April 1991 that increased the water pressure along discontinuity sets (Schindler et al. 1993, Sartori et al., 2003). Eberhardt et al. (2004) pointed out, by mean of hybrid geomechanical modelling, the influence between the pre-existing field conditions and the continuum degrading factor causing the progressive shear strength degradation. These authors also argue that it is not required to have fully persistent geological features to drive the failure.

2.3 Monitoring of the upper unstable area

The monitoring of the surrounding area of the Randa rockslide began just after the first rockslide event in April 1991. Until the second rockslide event (Mai 1991), 18 targets were installed and surveyed using Electronic Distance Meter (Ischi et al. 1991). After the second event, the destroyed targets were replaced and a total of 30 targets were monitored. Geodetic measurements were also carried out based on 14 reflectors between the two rockslide events and 19 reflectors after the second event. (Ischi et al., 1991, Rey and Rouiller, 1995). After the second event, the northern part of the rockslide scar still showed some instability evidences. In order to study the displacements in the upper part of the slope and to monitor the potential fracture opening, twenty-four extensometers (tape-measure) and five automatic extensometers were installed. In 1995, seven 3-D prism retro-reflectors were installed in order to describe the movements on the three axes (Jaboyedoff et al., 2004a, Ornstein et al., 2005). Since 2001, an important research project was conducted to improve the understanding of the kinematics of the potential instability created after the two main rockslide events based on new monitoring devices (including borehole inclinometers, extensometers and benchmark pairs) and geophysical investigations (Willenberg et al., 2008a, Willemberg et al., 2008b, Spillmann et al., 2007). Recently, new projects involving the use of modern monitoring techniques such as Ground-based InSAR (Gischig et al., 2009), and fiber-optic techniques (Moore et al., 2010) were tested.

2.4 Upper unstable area kinematics

The movement of the potential unstable area located in the upper part of the rockslide were firstly interpreted by Jaboyedoff et al. (2004a) based on the 1D displacements data. The proposed kinematics was a simple shear band affecting the slope in the direction 135/40, in agreement with the discontinuity sets defined by Sartori et al. (2003). Willenberg et al., (2008b) confirmed the presence of a planar shearing zone in the lower portion of the unstable area, based on 3D displacement data, geophysical investigations and borehole analyses. Nevertheless, this discontinuity was considered as not continuous. The same authors also argued for a block toppling to explain displacements direction in the upper part of the slope. Recently, Gischig et al. (2009) compared Ground–based InSAR data and geodetic distance measurements and confirmed the existence of a highly persistent basal rupture zone postulated by Jaboyedoff et al. (2004a).

3 DATA AND METHODS

3.1 New Available data

In 2008, an HRDEM of the entire rockslide area was acquired through a helicopter (resolution: 50 cm mesh size). This allows a detailed topographical characterization and a precise delimitation of the morpho-structural features. Satellites synthetic aperture radar (SAR) images of the Randa area were processed using the Local Permanent Scatter (PS) technique (TRE®, Ferretti et al., 2001) in order to detect permanent targets useful for the displacement monitoring. 51 SAR images from the satellites ERS taken in the ascending geometry and covering the period between May 1993 to July 2000 were used to determine the permanent scatters. The line of sight vector coordinates are N: -0.07993 E: -0.38993 H: 0.91737. Even if, the geometrical and topographical characteristics of the study area are difficult, 1516 permanent targets were identified, distributed mainly in the upper part of the slope. The

standard deviation on the velocity measurements is generally low, close to 0.2-0.5 mm/year, indicating the good consistency of the measurements.

3.2 Methods

Available data concerning the discontinuity sets orientation were assembled and visualized using stereographic techniques. The helicopter base point clouds were treated using the software COLTOP3D (Jaboyedoff et al., 2007). This software combines slope angle and slope aspect determined on grid data as well as unstructured point cloud data in a unique representation by mean of Intensity-Hue-Saturation system (IHS, see figure 2). In the case of steep rocky outcrops the slope angle and the slope aspect of the topography can be associated to the orientation of the discontinuity sets present in the area (Jaboyedoff et al., 2007). This software also allows an easy semi-automatic delimitation and extraction of the different potential discontinuity sets.

The volume calculation was performed using two different methods: the Sloping Local Base Level (SLBL) method and a 3D geometrical analysis of the helicopter-based point clouds, as follows (a) the SLBL method applied to a 3D surface consists of replacing the altitude z_{ij} of a DEM node by the mean value of the highest and the lowest node altitude among the four direct neighbors, only when the altitude z_{ij} is greater than the mean value (Jaboyedoff et al. 2009); (b) the geometrical analysis was performed using Polyworks (InnovMetric©) and consists in fitting planes along the main discontinuity sets in order to calculate the maximal volumes that could be mobilized. A simple geomechanical model using finite-element model was performed using the software Phase2 *(Phase2 code Rocscience©)* allowing introducing discontinuity sets. The parameters used are taken form the previous model performed in the same area (Eberhardt, 2004)

4 STRUCTURAL ANALYSIS

Structural analysis performed using COLTOP3D software allowed for the identification of 8 main discontinuity sets: J1, J2, J3, J4, J5, J6, J7 and J8 (Figure 3 Table 1). These results are consistent with previous fieldwork campaigns carried out by different authors (e.g. Wagner, 1991; Sartori et al. 2003; Willemberg, 2008a). Nevertheless, an additional highly persistent joint (J8), with a dip direction sub-parallel to the main foliation were also identified. This joint is mainly present in the upper portion of the slope and clearly influences the morphology of the western part of the slope (Light blue surfaces in Figure 2). In the same area, persistent lineation/faults parallel to J5 could be observed (Figure 2). Locally, an offset between 2 and 5 meters were measured. These structures are mainly visible on the Randa rockslide area and became difficult to follow along the North western side of the Mattertal valley.

The origin of these structures is unclear; they could be related either to a series of faults showing differential erosion or (more probably) to old gravitational movements related to the presence of a deep seated slope deformation (DSGSD) affecting the entire Randa slope. As suggested by Girod (1999), based on structural analysis performed in the by-pass tunnel, any joint could be clearly related to exfoliation phenomenon associated to the glacial unloading. However, we can assume an increasing persistence and opening of pre-existing joints sub-parallel to the main valley (J2, J5 and J6), after the last glaciations. The scar of the second rockslide event represents a classical example of structurally-controlled failure, especially in the south-eastern portion (Figure 2). The scar is delimited by three main planes: (a) a persistent J4 discontinuity set controlling the basal sliding surface; (b) J2 and J5 controlling the southern lateral surface, where a clear weathered surface indicates that water circulation an active process; (c) J4 and J6 control the stepped northern lateral/auxiliary sliding surface. The lateral extends and the mean block widths are controlled by J2 set. In this area, evidence of intact failure is present indicating a limited persistence of sliding planes.

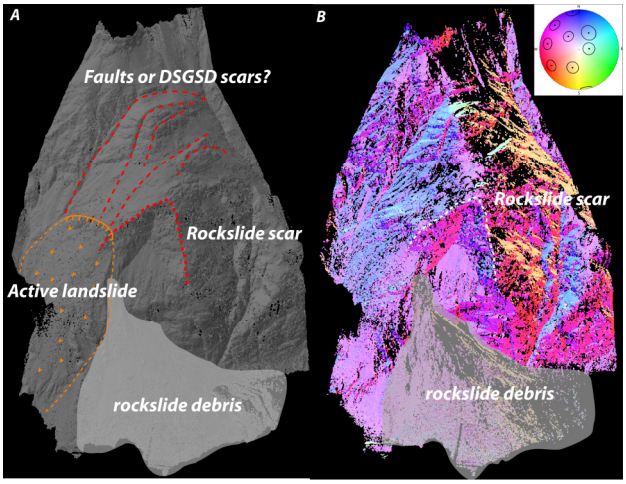

Figure 2. a) Hillshade 3D view of the Randa area showing the main morpho-structural features derived from helicopter-based point clouds. b) Visualisation of the same dataset by unique colour code (COLTOP 3D software) showing the significant structural control on the rockslide scar morphology.

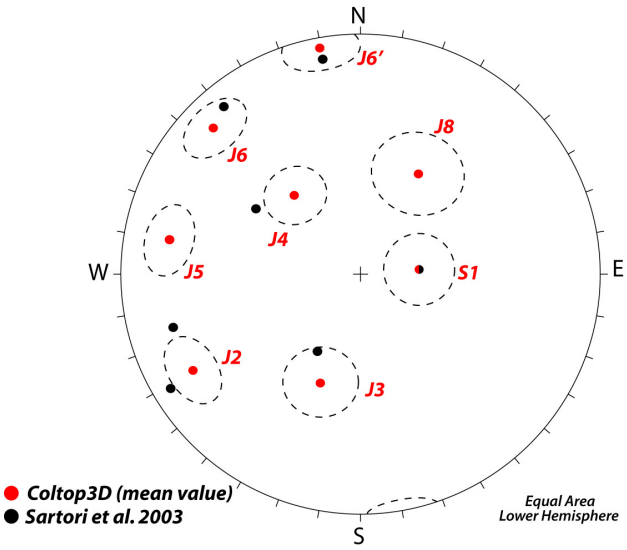

Figure 3. Stereoplot comparing the mean orientation of discontinuity sets detected on LiDAR point cloud using COLTOP 3D software (mean values red circles, 1 standard deviation dotted circles) and the mean values identified by Sartori et al., (2003) based on field observations.

Table 1. Characteristics of main discontinuity sets detected by COLTOP3D based on the helicopter point clouds.

Name (color, variation)	Dip direction	Dip	Relative distribution
S1 (green, +/-12°)	260	20	Whole area
J2 (Red+/-10°)	70	70	Central and lower area
J3 (Light-orange, +/-12°)	20	40	Whole area
J5 (Red-violet, +/-10°)	100	75	Whole area
J4 (Light violet, +/-10°)	140	35	Upper and central area
J6 (Violet-blue, +/-10°)	135	75	Central area
J6'(Dark blue +/-10)	170	85	Whole area
J8 (Light blue +/-15°)	210	40	Upper and central area

5 DISPLACEMENTS ANALYSIS

The detected permanent scatters (PS) were plotted on the high resolution orthophotos (see Figure 4). Only the points which velocity was over ± 2 mm/yr were plotted; this value is a significant threshold related to the technique precision. PS data of the Randa rockslide shows two areas with important negative velocities. Negative values indicate movements away from the sensor; based on the local geomorphological configuration, they could be interpreted as active gravitational movements. These two areas closely corresponds to the previously monitored upper unstable area (Jaboyedoff et al., 2004a) and to a sagging area located in the eastern part of the rockslide identified by Sartori et al., (2003). The upper unstable area shows differential displacement velocities reaching -12/-14 mm/y close to the rockslide crown area and decrease progressively to -4/-6 mm/y toward NNE (Figure 4a). The limit between the moving and stable areas is clearly visible in this figure, allowing for the delimitation of the potential unstable area.

As regards the sagging area, the presence of PS is mainly concentrated in the central portion of the instability. In this area, uniformly displacements velocities of about -6/-4 mm/y were measured (Figure 4a). In the lower portion of the instability, velocities decrease progressively to -4-/-2 mm/y. In the main scar area only few permanent scatters were detected, showing very slow displacements (-2/-3 mm/y). PSInSAR results of the rockslide crown area have been compared to previous geodetic measurements (Jaboyedoff et al., 2004,) and ground based SAR analysis (Gischig et al., 2009), indicating a good coherency in terms of mean velocities and extension of the moving area. The three methods indicate that the rockslide crown area shows the higher displacement velocities (12-17 mm/y). A progressive decreasing of velocities towards the rear part is also pointed out by the different data. It is important to remember that displacements derived from PSInSAR do not have the same orientation that displacements measured by geodetic method. The PSInSAR vector on which the velocities are projected plunges around 80° toward NE. In opposition, the geodetic vector plunges around 25° toward SE. Coupling the movements along these two vectors it is possible to calculate the "pseudo-real" displacement vector by solving the following equation system (Eq 1.)

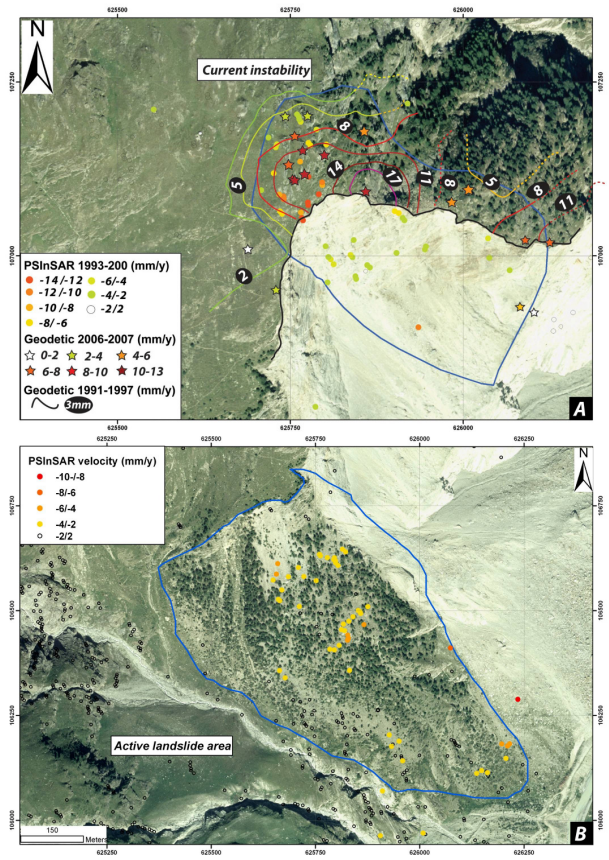

Figure 4. A) Comparison between geodetic monitoring displacement velocities (1991-1997 from Jaboyedoff et al., 2004a and 2006-2007 from Gischig et al., 2009) and PSInSAR velocities for the upper portion of the Randa rockslide. B) PSInSAR velocities in the landslide area located in the eastern part of the Randa rockslide scar. Velocities could reach -10/-8 mm/y in the central portion of the instability.

$$\begin{Bmatrix} \vec{PS} \\ \vec{Geo} \\ \vec{PS} \times \vec{Geo} \end{Bmatrix} \bullet \begin{pmatrix} x \\ y \\ z \end{pmatrix} = \begin{pmatrix} PSvel \\ Geovel \\ 0 \end{pmatrix} \qquad [1]$$

PS = PSInSAR line-of-sight unitary vector,
Geo = Geodectic line-of-sight unitary vector
PS x Geo = unitary cross product vector
The suffix *vel* indicates velocity along the related vector, *x, y* and z are the vector components of the displacement in the plane defined by the PS and Geo vectors.
Using this equation, any displacements outside of the normal plane of the two vectors is assumed. Hence, this estimation is a minimum displacement and does not correspond to the real 3D vector, but can be quite similar. For example, coupling PSInSAR and geodetic measurement between 2006 and 2008, for the frontal part, we obtained a vector plunging around 55° toward 124° with a velocity of about 17 mm/y. Similar results are obtained using the geodetic results covering the period 1991-1994. In order to analyze the possible orientation and norm variation of the real calculated vector, a sensitivity analysis was done by setting a non-zero displacement values along the cross-product direction in eq. 1 (Figure 5). The sensitivity analysis indicates that by adding positive or negative displacements, the plunge value is quite constant (between 55°-40°) but the trend shows more important variations (between 95°-180°). The normal vector does not change a lot, changing from a minimum of 17 mm/y to a maximum of 20 mm/y.

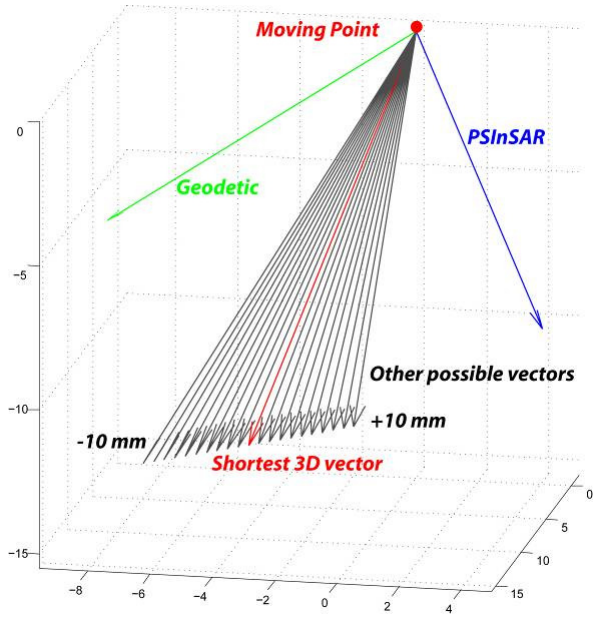

Figure 5. Example of a shortest 3D vector calculation using the displacements values of PSInSAR and geodetic sensors. These values correspond to the frontal portion of the unstable area. The variation of the orientation of the composed displacement vector is calculated by replacing the result of cross product in Eq. 1.

In order to analyze the variations of the shortest vector along the entire unstable portion, geodetic and PSInSAR data were interpolated for the monitored area following the methodology detailed by Jaboyedoff et al., (2004). Figure 6 shows the evolution of the calculated vector along a cross-section passing trough the unstable area. The trend of the vector remains quite constant along the unstable area; Nevertheless, the vector plunge decrease progressively from the frontal to the rear part (from 55° to 30°). The normal vector shows the same trend, decreasing progressively in the rear part of the instability.

6 MECHANISM REINTERPETATION

The structural setting corresponding to the current unstable area (upper part of the slope) is very similar to the structural setting of the 1991 second rockslide area.

Kinematics analyses performed using stereonet techniques indicate the possibility to have planar sliding along J4 and a potential wedges formed by J4^J2 with J6 and J5 acting as rear release surfaces. J2 set represents the main lateral release fracture.

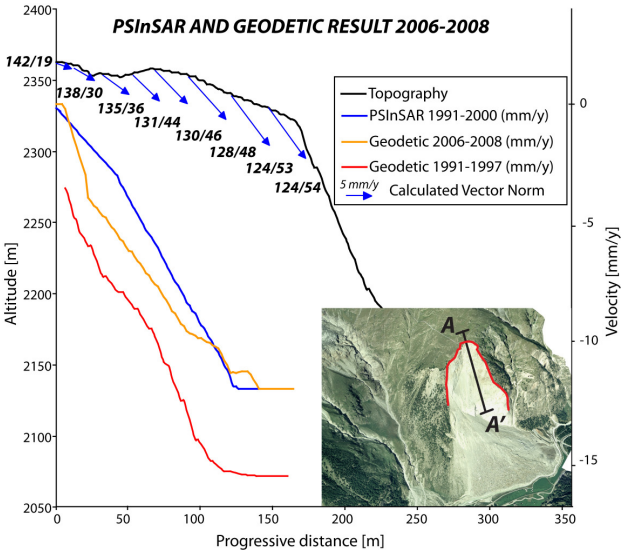

Figure 6. Variation of the shortest displacement vector calculated coupling the PSInSAR and geodetic velocities at different portion of the unstable mass.

The influence of these discontinuity sets on the failure kinematic have been previously proposed based on displacements analyses (Jaboyedoff et al., 2004a, Gischig et al., 2009). The general kinematics of the entire unstable area is probably controlled by a stepped planar sliding formed by J4 and J6. However, the important movements detected by PSInSAR analysis along the line of sight, suggest that significant sub-vertical movements occurs in the upper unstable area. In this area, the presence of several open cracks with different orientations indicates also a more complex behaviour. Figure 7 shows the possible values of the calculated displacement vectors by adding negative or positive displacements of the normal direction of the plane formed by the PSInSAR and geodetic vectors. In the same figure, the dip angle and dip direction of the main important discontinuity sets are reported. It is possible to see that, by adding displacements along the normal of the plane constructed by PSInSAR and geodetic vectors, the calculated vector reaches the same trend than discontinuity sets J4 and J6, suggesting and clear influence of this discontinuity on the failure kinematics. However, by adding the same displacements the calculated vector plunge is not comparable to the dip of the two main discontinuity sets involved in the stepped planar failure. This indicates that more complex kinematics mechanism affects the entire unstable area. In fact, if only planar sliding kinematics was active, the plunge of the calculated vector will be closer to the flatter discontinuity set J4. To explain the calculated plunge values, an important vertical component affecting the entire upper unstable area need to be integrated in the kinematical model.

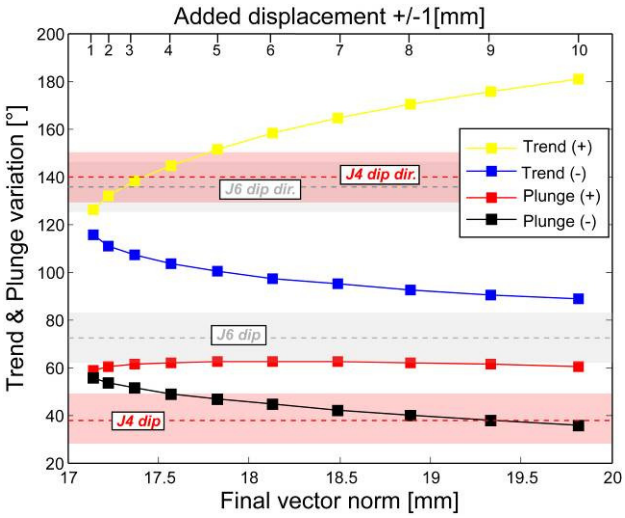

Figure 7. Comparison between the calculated trend/plunge of the vector and the orientation of the main important discontinuity sets limiting the potential failure surface.

Based on displacement measurements, the observed vertical movements are higher in the frontal portion of the instability and progressively decrease in the rear portion. These vertical moments could be related to the important fracturing of the unstable area and, as suggested by Willemberg et al., (2008b), to the presence of densely spaced discontinuity sets plunging into the slope together with cutting discontinuity sets dipping gently out of the slope. The presence of these two characteristics in the upper area leads to expect the presence of several small rigid blocks delimitated by persistent discontinuities and intercalated by rare rock bridges. Shear movements along sub-vertical sets and progressively rock bridges failures coupled with a deeper stepped planar sliding will probably explain the important sub-vertical component of the instability's kinematic. Figure 8 shows the conceptual model of the upper unstable area presenting the relations between the upper fractured area and the stepped deeper failure surface. In order to validate this conceptual model and to predict the movements detected along the geodetic vector a simple geometrical model coupling the PS movements with a steep discontinuity set and the basal failure surface have been carried out. Figure 8 resumes the geometrical specifications and the results of the model. It is interesting to note that this simple failure predicts in a good way the general displacement trend observed by geodetic measurements. In addition the model confirm the important influence of shearing movements along sub –vertical discontinuity sets leading to more steeper total displacement vector.

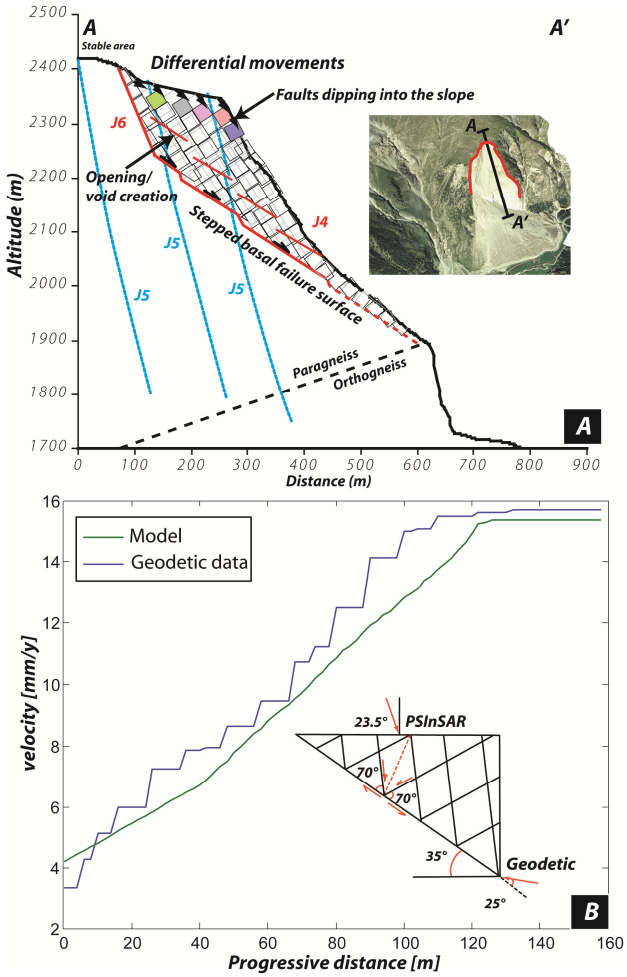

Figure 8. A) Schematic cross-section showing the potential kinematic of the upper unstable area. For the deeper movements a stepped planar failure is proposed. B) Geometrical model coupling PSInSAR velocities and main structural setting through the upper unstable area to predict the displacements along the geodetic vector.

To test the validity of the proposed geometrical model, especially the calculated displacements direction (Figure 6) in a more quantitative way, a finite-element model *(Phase2 code Rocscience©)* was produced. Discontinuity sets, rock mass parameters and in-situ stress were derived from previous geomechanical model performed on the area (Eberhardt et al., 2004). We modeled the rock mass using elastic properties and we introduced a progressive shear strength reduction of the joint cohesion. The potential lower failure surface and the main discontinuity sets affecting the frontal unstable area were explicitly introduced in the geomechanical model. Also in this case, the results show the same trend as the geometrical model. The norms of displacement vectors as well their inclination decrease progressively toward the rear portion of the instability. Inside the unstable mass important extensional movement and crack open have also been observed (Figure 9).

Concerning the landslide area located in the southern portion of the Randa rockslide, only displacements data based on PSInSAR analysis are available. The Permanent Scatters are mainly concentrated in the central and in the lower portion of the area. Any point was detected in the upper portion. The important movements detected using this methods (reaching locally 10mm/y) confirm the presence an active landslide area of about 0.47 km^2. Clear sign of gravitational movements are visible in the upper part of the slope (cracks scarp and counterscarps) and also at the southern margin of the Randa rockslide (Figure 10).

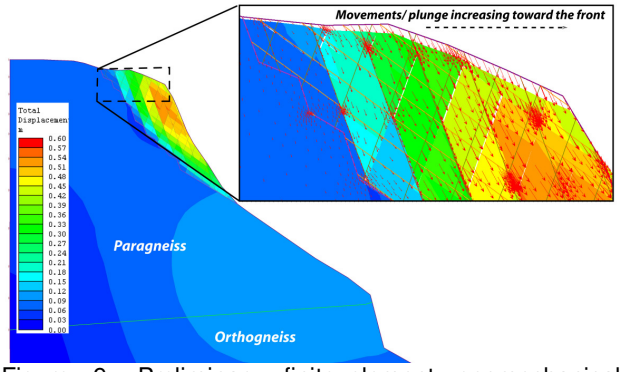

Figure 9. Preliminary finite–element geomechanical model showing the total displacement on the upper instability. The displacement directions are in agreement with the movement directions observed by geodetic and PSInSAR analysis together with the proposed geometrical model of the figure 8.

In this area, the lower shearing surface outcrops directly on the Randa rockslide scar. Preliminary structural observations indicate that the potential kinematics of this area is a stepped planar failure involving discontinuity sets J8 and J6'. Like illustrated in Figure 10A, it is not possible to point out a unique well-defined failure surface. Nevertheless, a 15-20 m large band, with low the rock mass quality is visible. This disturbed area corresponds probably to the location of the multi-step failure zone (Cf. Figure 10B).

7 UNSTABLE VOLUME ESTIMATION

The geometrical reconstruction using the HRDEM allows delimiting a maximal potential unstable volume using two parameters: (a) discontinuity sets orientation and (b) extension of the moving area detected by PSInSAR. A maximal unstable volume of 4M m^3 was calculated (Figure 11). The SLBL method allows disposing to another estimation of the potential unstable volume. The SLBL calculation was constrained using the instability limits and the dip of the lower sliding surface as invariant points. An angle of 35° was used to delimit the lower sliding surface. The SLBL result indicates a potential unstable volume of varying between 3.5-3.7 M of m^3

depending on the applied tolerance. A difference of about 15% between the two methods can be pointed out. This difference is probability related to the fact that using geometrical construction we do not account for large scale undulations of the main discontinuity sets or failure on rock bridges.

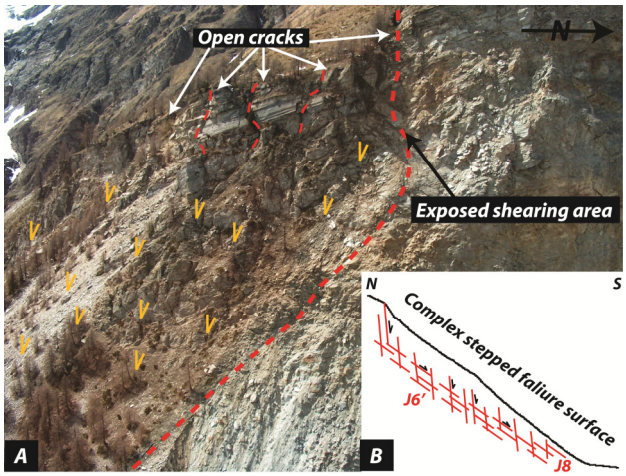

Figure 10. A) Oblique view of the upper portion of the landslide area located in the southern part of the Randa rockslide. A large portion of the multi-step shearing surface delimiting the basal sliding area is delimited with a discontinuous line. B) Schematic cross-section of the sliding area showing the complex stepped sliding area.

SLBL created a curved surface approaching better complex and stepped failure surface. The estimated volumes are 20-25% lower than the volumes estimated by Gischig et al., (2009). This difference is probably related to a better instability delimitation base on LiDAR point clouds information.

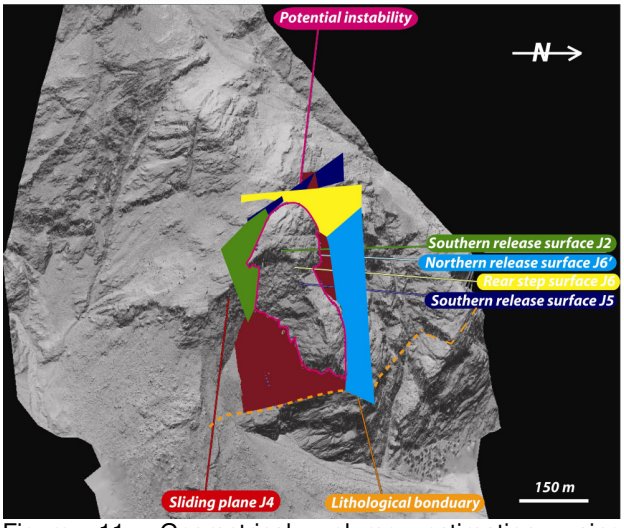

Figure 11. Geometrical volume estimation using helicopter-based point cloud and calibrated on main discontinuity sets orientation and persistence.

8 CONTRIBUTION OF THE NEW AVAILABLE DATA

The new available data presented in this paper allow progression of the comprehension of the Randa rockslide area in term of mechanism and present-day activity. The treatment of the helicopter-based point cloud allows identifying new discontinuity sets influencing the stability and the morphology of the entire slope. In addition, based on persistent structures detected in the upper portion of the slope, the presence of a potential, probably inactive DSGSD, is postulated.

PSInSAR analysis shows that important displacements occur in the upper unstable area but also in the southern landslide area. The detected velocities are comparable with the other monitoring techniques.

The kinematics of the upper instability was better constrained, especially in terms of involved discontinuities. Previous postulations of a planar sliding on J4 seem to be verified especially concerning the deeper movements. The current real kinematics at the upper portion of the unstable area still remains very complex, involving progressive rock bridges failure and shearing movements along persistent discontinuity sets.

Finally, it was possible to describe the general trend of the measured displacement vectors by coupling the different available displacements data and the main discontinuity sets. Nevertheless, more 3D displacement datasets are need to better constraint the different movements directions detected by previous studies. .

ACKNOWLEDGEMENTS

The writers would like to thank Pascal Horton for their comments and suggestions. This research has been supported by the Swiss National Found (grant number 200021-118105) and by Herbette Foundation. We also thank the CREALP and its director J.-D. Rouiller.

REFERENCES

Bearth, P. 1964: Geologischer Atlas der Schweiz, Blatt N 1328 Randa mit Erklärungen, Schweizerische Geologische Kommission.

Eberhardt, E., Stead, D., and Coggan, J. S.. 2004 Numerical analysis of initiation and progressive failure in natural rock slopes–the 1991 Randa rockslide, *Int. J of Rock Mech. Min.*, 41, 69–87.

Ferretti A, Prati C, Rocca F (2001) Permanent Scatterers in SAR Interferometry. IEEE *Trans. Geoscience And Remote Sensing* 39(1): 8–20.

Girod, F.1999. Altération météorique de roche granitique en milieu alpin: le cas de l'orthogneiss associé à l'´eboulement de Randa (Mattertal, Valais, Suisse). PhD Thesis, Université de Lausanne.

Gischig, V., Loew, S., Kos, A., Moore, J. R., Raetzo, H., and Lemy, F. 2009. Identification of active release planes using ground-based differential InSAR at the Randa rock slope instability, Switzerland. *Nat. Hazards Earth Syst. Sci.*, 9, 2027–2038.

Götz, A. and Zimmermann, M. 1993. The 1991 rock slides in Randa: causes and consequences, *Landslide News*, 7/3, 22–25.

Ischi, H., Keusen, H. R., and Scheller, E.1991. Randa Kt. Wallis. Bergsturz Grossufer vom April/Mai 1991, Zusammenfassender Bericht ¨uber die Aktivit¨aten der Geotest AG., unpublished report 91126 Geotest AG, Martigny.

Jaboyedoff, M., Ornstein, P., and Rouiller, J.-D. 2004a Design of a geodetic database and associated tools for monitoring rock-slope movements: the example of the top of Randa rockfall scar, *Nat. Hazards Earth Syst. Sci.*, 4, 187–196.

Jaboyedoff, M., Baillifard F., Bardou E, and Girod F. 2004b: Weathering, cycles of saturation-unsaturation, and strain effects as principal processes for rock mass destabilization. *Quarterly Journal of Engineering Geology and Hydrogeology*.

Jaboyedoff, M., Metzger, R., Oppikofer, T., Couture, R., Derron, M.-D., Locat, J., and Turnel, D. 2007. New insight techniques to analyze rock slope relief using DEM and 3D-imaging cloud points: COLTOP-3D software, in: *Rock Mechanics: Meetings Society's Challenges and Demands*, edited by: Eberhardt, E., Stead, D. and Morrison, T., Taylor & Francis, 1: 61-68.

Moore J. R., Gischig V., Button E., and Loew S. 2010. Rockslide deformation monitoring with fiber optic strain sensors. *Nat. Hazards Earth Syst. Sci.*, 10, 191–201

Noverraz, F. and Bonnard, C. 1992. L'écroulement rocheux de Randa, près de Zermatt, in: Landslides, Proceedings of the 6th International Symposium, Christchurch, edited by Bell, D. H., Balkema, Rotterdam, 1, 165–170.

Pirocchi, A. 1992. Laghi di sbarramento per frana nelle alpi: tipologia e evoluzione, Tesi di dottorato, Università di Pavia, Pavia, 155.

Sartori, M., Baillifard, F., Jaboyedoff, M., and Rouiller, J.-D. 2003. Kinematics of the 1991 Randa rockslides (Valais, Switzerland), *Nat. Hazards Earth Syst. Sci.*, 3, 423–433.

Spillmann, T., Maurer, H. R., Heincke, B., Willenberg, H., and Green, A. G. 2007. Microseismic monitoring of an unstable rock mass, *J. Geophys. Res.*, 112, B07301.

Schindler, C., Cuenod, Y., Eisenlohr, T., and Joris, C.-L. 1993. Die Ereignisse vom 18 April und 9 Mai 1991 bei Randa (VS) – ein atypischer Bergsturz in Raten, *Eclogae geol. Helv.*, 86/3, 643–665.

Wagner, A. 1991. Bergsturz Grossgufer Randa, étude structurale et gémecanique, Unpublished report number 91, 35, CRSFA, Sion, 16p and annexes.

Willenberg, H., Loew, S., Eberhardt, E., Evans, K. F., Spillmann, T., Heincke, B., Maurer, H., and Green, A. G. 2008a. Internal structure and deformation of an unstable crystalline rock mass above Randa (Switzerland): Part I–Internal structure from integrated geological and geophysical investigations, *Eng. Geol.*, 101, 1–14.

Willenberg, H., Evans, K. F., Eberhardt, E., Spillmann, T., and Loew, S. 2008b Internal structure and deformation of an unstable crystalline rock mass above Randa (Switzerland): Part II–Three-dimensional deformation patterns, *Eng. Geol.*, 101, 15–32.